NZGS SYMPOSIUM 2021
Good grounds for the future
24-26 March 2021 • Dunedin • New Zealand

Simulation of piles subjected to excavation or embankment loading

W. D. Guo
TBA, Brisbane Australia

ABSTRACT

This paper provides investigation into response of (forward-rotated or backrotated) piles subjected to embankment loading, in light of 2-/3-layer models. First, recent advance is briefly reviewed concerning range of parameters used to model piles subjected to excavation and embankment loading. Second, simulations of six centrifuge tests on embankment piles are exemplified. Third, 1g model tests are provided to reveal backrotation behaviour of piles, and its simulation. The study is aimed to unite the design of piles under various types of passive loading (e.g. lateral spreading, embankment, excavation, sliding slope, etc.)

1 INTRODUCTION

Numerical analysis indicates the challenge in gaining parameters to achieve reliable prediction of the pile response affected by excavation, and embankment loading. For instance, the on-pile pressure from centrifuge tests on piles subjected to lateral spreading is reportedly quite close to the residue strength for liquefied sand (Armstrong et al. 2014), but is sometimes inconsistent with JRA (2002) methods. The prevalent *p-y* curve based methods are not suitable for modelling piles subjected to lateral spreading against 3D numerical analysis, although modifying the residual strength and stiffness of the p-y curve improve the prediction.

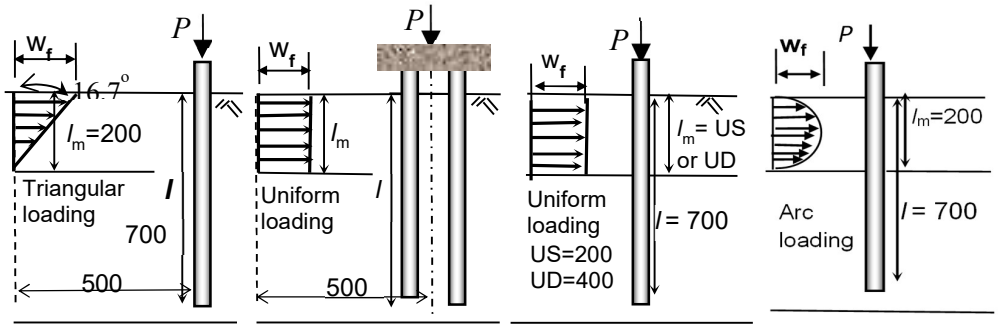

Figure 1: Tests on piles under an inverse triangular, uniform or arc profile of soil movement

Recently, Guo (2015, 2016) developed 2- and 3-layer theoretical models and the associated closed-form solutions. The solutions well capture nonlinear response of piles in sliding soil [e.g. lateral spreading (Dobry et al. 2003), sliding sand (Guo et al. 2017; see Fig. 1), and slope (Frank & Pouget 2008)]. In particular, the same set of input parameters well capture the 3–5 times higher bending moment induced under translational movement than rotational movement, which is not seen in other simulations. This prompts the use of the models to capture impact of embankment or excavation loading on piles.

2 2-/3-LAYER MODELS AND SOLUTIONS

Rigid passive piles are simulated for a stepwise, uniform soil movement w_s (thus external loading p_s of $w_s k_s$, k_s is modulus of subgrade reaction) to a sliding depth l_m [see Fig. 2]. A fictitious layer is introduced to account for dragging above the underlying stable layer, and forms a 3-layer model [see Fig. 2, Guo (2016)]: a sliding layer with the modulus k_s (depth $0 - l_m$), a transition (fictitious) layer with a linearly increasing modulus from the k_s at depth l_m to mk_s at the depth z_m of maximum bending moment M_m, and a stable layer with a modulus mk_s in depth z_m–l (l = pile embedment), respectively. Without the transition layer, the model is referred to as 2-layer model (Guo 2015). Under a rotational restraining stiffness k_θ, and a lateral force H, the pile rotates rigidly about a depth z_r to an angle ω_r and a mudline deflection w_g under the sliding movement w_s, or on-pile **f**orce **p**er **u**nit **l**ength (FPUL) p_s [$= \alpha p_{ub} l_m / l$, and $p_b = \alpha p_{ub}$], to a sliding depth of l_m on the pile. As shown elsewhere, the l_m is equal to $(0.6–3)l_{exc}$ for an excavation depth l_{exc}, for a distance between excavation face and piles of about $0.25l$. The model is underpinned by the five input parameters k_s, m, p_b (FPUL at pile-base level), k_θ, and a factor α of non-uniform soil movement.

Explicit expressions were developed to estimate the displacement $w(z)$, shear force $T(z)$ and bending moment $M(z)$ at depth z, the maximum bending moment M_m, its depth z_m of M_m and the maximum shear force T_m (sliding or stable layer). The solutions are repeated for a series of l_m/l (e.g. raising by a step of 0.1) and $p_s = p_b l_m / l$ until a final $l_m/l = 0.5–0.9$ to gain nonlinear response (Guo 2015). It should be stressed that the solutions are contemplated for rigid piles with rotational stiffness k_θ, $k_{\theta G}$, and $k_{\theta T}$, otherwise other solutions (e.g. Poulos and Davis 1980; Guo 2012) should be consulted.

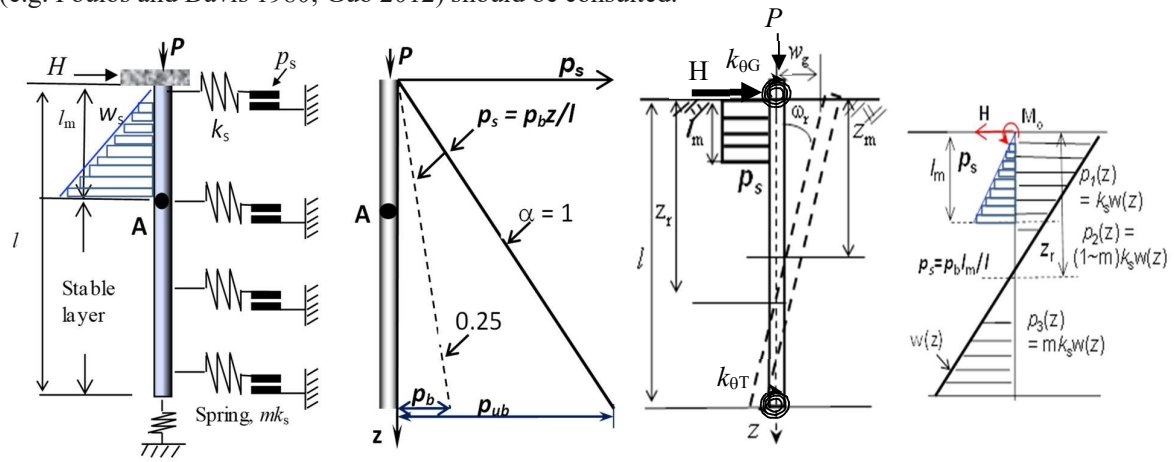

Figure 2: Models for rigid, passive piles: model, p_b and p_{ub}, k_θ, and p_s for nonlinear response

3 MODELLING PILES SUBJECTED TO EXCAVTION OR EMBANKMENT MOVEMENT

The 2-layer and 3-layer models are adopted to simulate the response of piles in ten model tests, subjected to excavation (Fig. 3, e.g. Leung, et al. 2000; Ong, et al. 2006) or embankment loading (e.g. Stewart et al. 1994; Armstrong et al. 2014). Typical parameters [of FPUL p_{ub}, modulus of subgrade reaction k_s, modulus ratio of stable over sliding layers m, and rotating stiffness k_θ] are deduced against measured piles response. The study

reveals that (1) The k_s reduces from 225s_u (stable piles, s_u= undrained shear strength) to (55–130)s_u (collapsed piles) due to increasing soil deformation from adjacent excavation. It is about 2.8N or 6z (MPa, N = SPT blow counts, and z = depth, m). Only (0.1–1.0)% k_s (of excavation loading) is noted for consolidating and lateral spreading embankment. (2) Normalised by overburden stress (σ_v'), pile width (d) and coefficient of passive earth pressure (K_p), the ratio $p_{ub}/(K_p\sigma_v'd)$ is deduced as 0.26–0.41 or 0.8–1.1 for embankment underlain by thick-clay layer or laterally spreading, and by clay-sand layers, respectively. (3) Excavation induces deformation of soil to a depth of 1.08αl_{exc}, and on-pile FPUL p_s (= $\alpha p_{ub} l_{exc}/l$). The evolution of wall collapse from stable wall is associated with increasing deformation zone (with α raising from 1.2–2.3 to 2.5–2.9), friction angle of soil sliding [from (0.61–0.65)ϕ' to (0.65–0.83)ϕ', ϕ'= angle of internal friction] and ratio of rotational resistance (modulus) m (from 2.7 to 4) at constant loading depths for clay-sand layers. The stress reduces by 50% (with α = 0.63–1.1 and m = 1.4) for piles in a single sand layer but for a high stiffness (k_s = 4.3 MPa). (4) Consolidating embankment involves a residual p_{ub}, smaller dimension and stiffness (with α = 0.5–0.72, k_s = 15–20 kPa) but larger rotational resistance (m = 17.7) than that induced by excavation loading (of α = 1.2–2.9, k_s = 0.55–2.25 MPa, and m = 2.9–4.0); and finally (5) The α (= 0.9–1.3), m (= 5.2–9.0), and k_s (= 26–80 kPa) of laterally spreading sand-embankment sit in between consolidating embankment and excavation loading. Response of flexible piles is well captured using the 2-layer model (for rigid piles) and modified k_s, p_{ub} and m values of (1.2–3)k_s, and (–0.8)p_{ub} and(–0.8)m. The impact of pile flexibility is also assessed using new models incorporating hinges of rigid piles. The new findings are useful to design of piles, regardless of which methods. Typical examples are provided next for modelling pile response subjected to embankment loading.

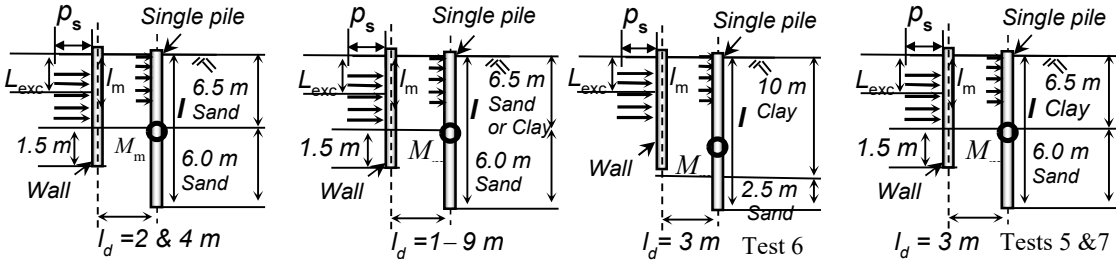

Figure 3: Centrifuge tests on piles (behind wall) subjected to excavation in sand or clay-sand layer

4 PILES SUBJECTED TO LARGE EMBANKMENT MOVEMENT

Given potential dragging' on the piles, the 3-layer model is adopted to analyse centrifuge model tests on pile groups either subjected to 'static' embankment loading (q), or spreading of sand embankment.

4.1 Piles nearby embankment

Stewart, et al (1994) conducted centrifuge tests on model pile groups, which consisted two rows of seven piles held in a rigid cap 2 m (all at prototype scale) above the soil surface and able to deflect freely. The piles penetrated through a soft clay layer and into an underlying dense sand stratum. Next to it, a sand embankment was constructed in six stages to a height of ~ 8.5 m (maximum). Four piles (22.5 m in length, 0.43 m in diameter) were instrumented in the pile group. Two typical Tests 9 and 11 are simulated herein.

In Test 9, the soft clay layer was 18-m thick, and had an average s_u of 17 kPa. The pile-cap displacement w_g (front/back row) and maximum moment M_m (both rows) were measured and are shown in Fig. 4(a) and (b), respectively for the increasing embankment height (or the average vertical stress q). The measured moment M_m is plotted in Fig. 4(c) against the pile-cap displacement w_g for both rows. The measured bending moment profiles with depth at 'ultimate' state are depicted in Fig. 4(d) for front- and back-row piles. The piles (l = 22.0 m, d = 0.43 m) are simulated using following parameters: p_{ub} = 51 kN/m [= $4s_u dl/(0.82l_m)$, with s_u = 17 kPa, d = 0.43 m, and l_m = 18 m], m =17.7 (= ratio of coefficient of passive earth pressure K_p [= $\tan^2(45+0.5\phi)$] over the active one K_a [= $\tan^2(45-0.5\phi)$]) at ultimate state], $k_\theta = k_G$ = 1.12 MN·m/radian (with

$\bar{k}_\theta$ = 0.007, G = ground level), and α = 0.5 (deep sliding) (see Fig. 4(a)). Given ϕ' = 23°, γ' = 16.5 kN/m^3, and l_m = 0.5l = 11 m, and q = 100 kPa, it follows an average p_s of 34.2 kN/m (= 51α), and $p_{ub}/(\sigma_v' d)$ = 0.72.

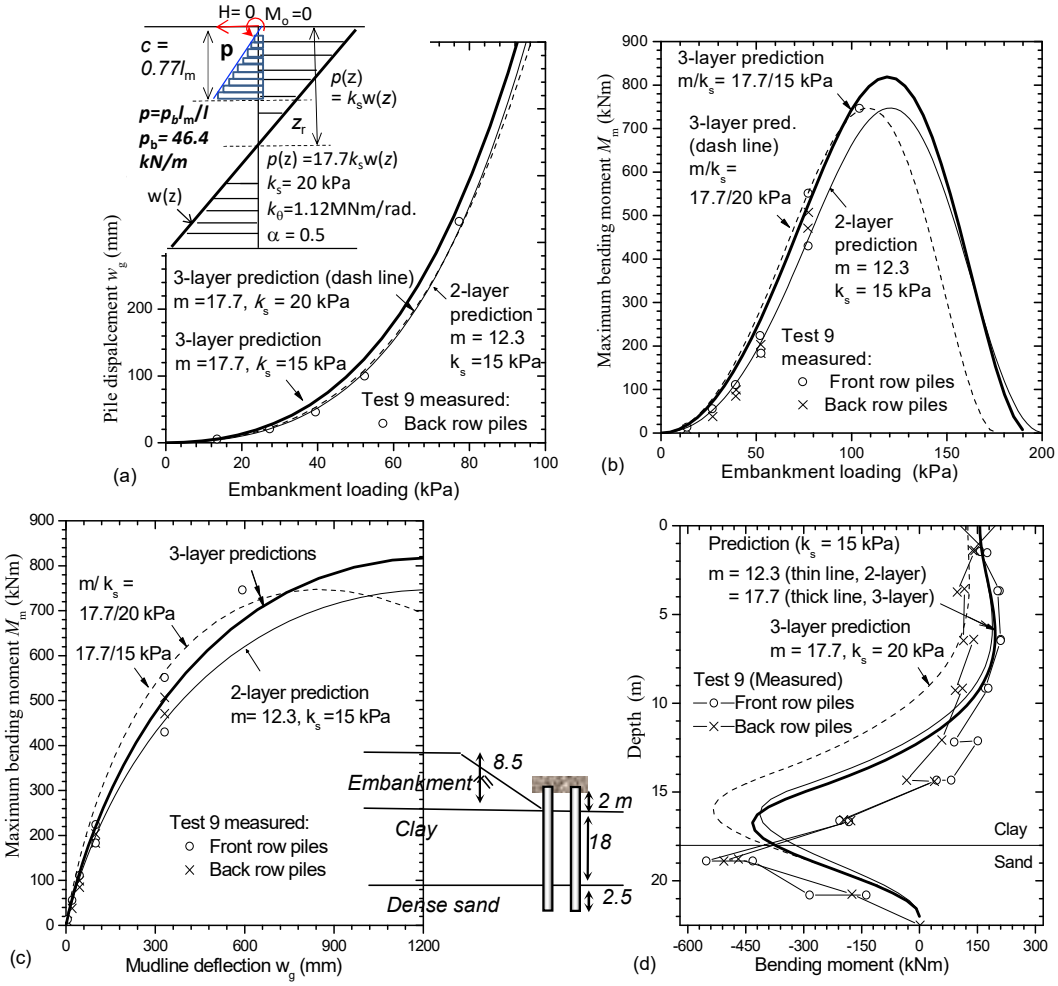

Figure 4: Predicted versus centrifuge Test 9 (Stewart et al. 1994): (a) embankment load versus maximum bending moment, (b) embankment load versus pile-head deflection, (c) pile-head deflection versus maximum bending moment, (d) bending moment profiles

The corresponding $p_s/(dq)$ = 0.72 (for over-consolidated clay) is slightly smaller than 0.75–0.792 deduced from measured response of piles subjected to short-term embankment loading, but is much higher than $p_s/(dq)$ = 0.277–0.35 for long-term embankment loading (Jeong et al. 1995). The $p_s/(\sigma_v' dK_p)$ is equal to 0.286. The previous study (Guo 2016) indicates k_s (= 15~20 kPa) and m = 12.3 (2-layer) or 17.7 (3-layer). The q-w_g, q-M_m, and w_g-M_m curves were thus predicted, and are shown in Fig. 4, along with the measured data. The 'limiting' bending moment profile was predicted for a loading depth c of 14.7 m (= 0.81l_m, l_m = 18 m), as plotted in Fig. 4(d). The predictions are insensitive to the modulus k_s, and indicate 50% (α = 0.5) surcharge loading q being transferred onto the on-pile pressure (= p_s/d) for the deep sliding. The k_s may also be obtained using the scant modulus G_{sec}= 60s_u[1-0.985(c/l_m)$^{0.2}$] (Stewart et al. 1994), assuming a maximum shear stress mobilization ratio of c/l_m. At c/l_m= 0.82 with s_u= 17 kPa, it follows G_{sec} = 54.4 kPa, and k_s = 18.1 kPa {= G_{sec}/[2(1+0.5)], Poisson's ratio = 0.5}.

In Test 11, the clay layer was 8-m-thick with s_u = 11 kPa. The piles (with l = 22.0 m, d = 0.43 m) are modelled using p_{ub} = 121 kN/m (= 3.1$s_u d l_m$, with s_u = 11 kPa, d = 0.43 m, and l_m = 8 m), k_s = 20 kPa, m =17.7, k_θ = 26.6 MN·m/radian ($\bar{k}_\theta = \bar{k}_A$ = 0.15 for the pile-cap), and α = 0.72 (a profile of inverse triangular

movement). The p_{ub} offers an average p_s of 86 kN/m (= 121α), $p_{ub}/(d\sigma_v')$ = 1.5–2.1 and $p_{ub}/(\sigma_v' dK_p)$ = 0.68–0.93 (with ϕ' = 23°, γ' = 16.5 kN/m^3, and l_m = 8–11 m). The normalised rotational stiffness $\bar{k}_\theta$ was raised to 0.15, due to a higher impact of underlying sand layer on the soft clay layer. These parameters allow a good prediction of q-w_g, q-M_m, and w_g-M_m curves (not shown herein). As a comparison, the 2-layer predictions were made using the same parameters (but for a reduced m of 12.3), which agree well with the measured data, respectively.

4.2 Piles embedded in lateral spreading embankment

Three centrifuge tests (Armstrong et al. 2014) were conducted to examine the response of embankment-pile subjected to lateral spreading. Each test comprised of two identical approach embankments (of dry, dense Monterey sand, D_r = 100%), which are separated by a 12-m wide channel. The embankments were 8 m high at the crest and 11 m high at the model container wall (or an average of 10 m in current modelling), with a crest width of 12 m and side slopes of 2:1 (horizontal to vertical) in all directions. Below the embankment was a compacted, non-plastic silt layer 1.3 m thick, a 5-m-thick loose sand layer (D_r =30%), a second silt layer 0.7 m thick, and a 17-m-thick, dense sand layer (D_r = 75%). One embankment from each centrifuge test (referred to as Kobe-1×6, Kobe-2×4, and Sine-2×4) included a pile group that extended into the dense sand layer. The Kobe-1×6 test was conducted on a single row of six closed-ended, aluminium piles with an outer diameter of 0.72 m and a flexural stiffness (EI) of 174 MN·m^2. The Kobe-2×4 and Sine-2×4 group tests both had two rows of four closed-ended, aluminium piles, with d_o (outside diameter) = 1.22 m, a center-to-center spacing of 3d_o, and EI = 1,876 MN·m^2. An aluminium-epoxy pile cap connected the piles together in each test. Input motions were applied to the model base in the longitudinal direction. Model Kobe-1×6 and Kobe-2×4 tests were subjected to a modified version of the ground motion recorded at a depth of 83 m at Port Island in the 1995 Kobe Earthquake, with a peak base acceleration of 0.8g and 0.7g, respectively. Model Sine-2×4 was first subjected to a shaking event contained a total of 20 sine wave cycles with packets at 0.2g, 0.3g, and 0.5g, respectively.

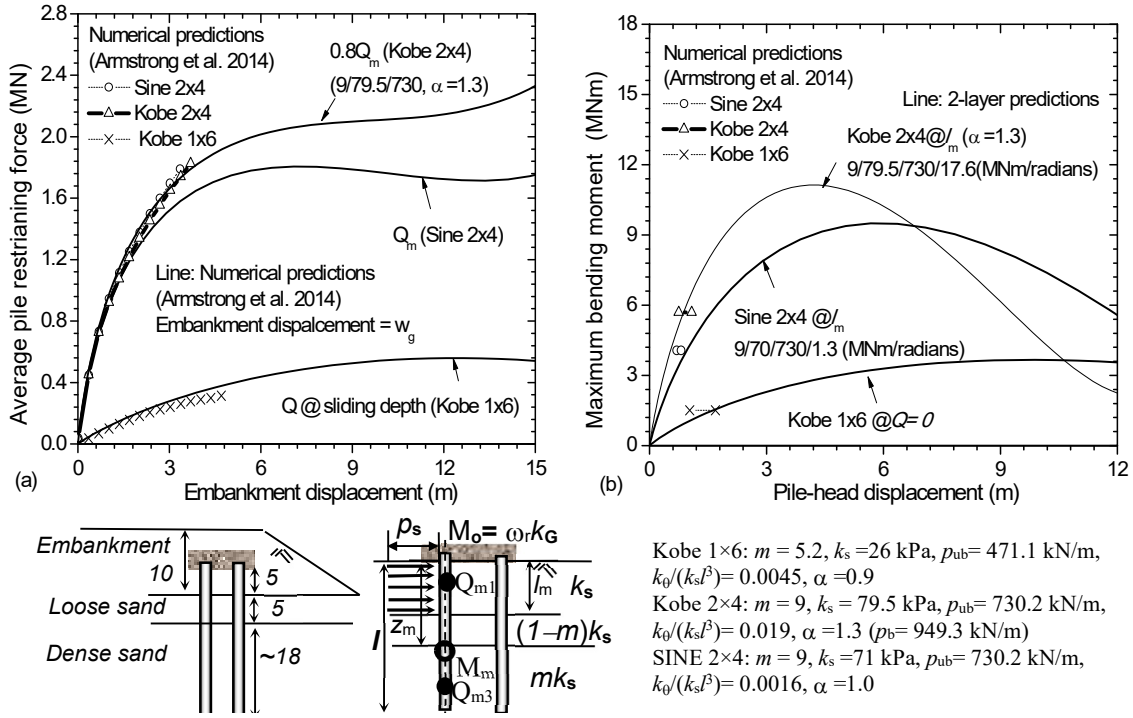

Figure 5: Predicted versus numerical solutions (Armstrong et al. 2014) of (a) maximum shear force versus embankment displacement, and (b) maximum bending moment versus pile-head deflection

An equivalent static analysis (ESA) was conducted on the centrifuge tests to gain in sequence (1) the

embankment displacement and displacement profile for a range of pile/bridge restraining forces, (2) the pile/bridge restraining forces for a range of imposed ground displacements, and (3) the point of compatibility in the forces and displacements between the two steps. The analysis overestimated the embankments deformations (without piles) (Armstrong et al. 2014), and bending moment of the piles (Fig. 5) against the centrifuge tests. It is thus important but difficult to select input parameters (e.g. undrained shear strength).

In simulating the piles of Kobe 2×4 test, the 3-layer solutions adopt: p_{ub} = 730.2 kN/m, m = 9 (ϕ' = 30°), k_s = 70.5 kPa [= 51d1.5m(l_m/l)^{2}1.5, d = 1.22 m], and k_θ = 1.3 MN·m/rad (see Fig. 5). The surcharge q was calculated for the embankment height h_e of 8 to 11-m (above the loose sand). The lateral spreading FPUL p_s was estimated as 162.26 kN/m (= 0.78$\sigma_v'd$, with σ_v' = $\gamma' h_e$, γ' = 17 kN/m^3, and h_e = 10 m) in light of $p_s/(\sigma_v' dK_p)$ = 0.26 (with ϕ' = 30°). The normalised on-pile pressure $p_s/(dq)$ is estimated as 0.78, as with short-term embankment loading (Jeong et al. 1995). The p_{ub} is obtained using l = 22.5m, l_m = 5 m, and α =1.0 with $p_{ub}/(\sigma_v' d)$ = 0.6. The current predictions agree well the numerical solution of restraining force–embankment displacement relationship, and pile-head displacement – maximum bending moment curve, respectively in Fig.5; and (2) the profiles of bending moment in Fig.6.

As with Kobe 2×4, the groups Kobe 1×6 and Sine 2×4 were simulated and shown in Fig.5. A design level of m = 5.2 (about 60% ultimate value of 9) was adopted for the Kobe 1×6 to compensate the impact of flexibility associated with the small diameter. A similar ratio $p_s/(\sigma_v' dK_p)$ of 0.28 (based on /(σ_v' = 170 kPa and ϕ' = 30°) [or $p_{ub}/(d\sigma_v')$ = 0.66] was adopted, which offers p_s = 105.3 kN/m (Kobe 1×6) and 176.3 kN/m (Sine 2×4), respectively. The current predictions agree well the numerical solutions. The pile-head displacement (at c = l_m = 5 m) is predicted as 1.05 m (Kobe 1×6), 0.75 m (Kobe 2×4) and 0.56 m (Sine 2×4), which agree well with measured values of 1.03 m, 0.75 m and 0.57 m, respectively. The agreement is observed (Fig. 6) for the profiles of bending moment as well. The current solutions are much simple and efficient to apply than other approaches, and have a good accuracy. Note that the stipulated α value can only be verified with evolution of the pile response with the soil movement, which is not available

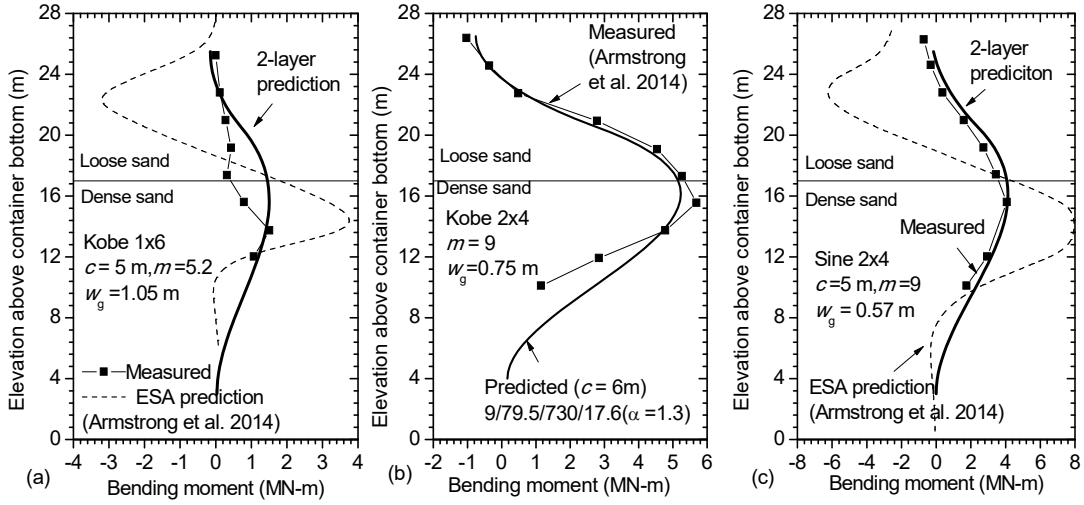

Figure 6: Predicted versus measured (Armstrong et al. 2014) bending moment profiles at a pile-head displacement of (a) 1.03 m (Kobe 1×6), (b) 0.75 m (Kobe 2×4) and (c) 0.57 m (Sine 2×4)

5 PILES SUBJECTED TO BACKROTATION

The existing tests, analytical and numerical simulations have been confined to forward rotation (e.g. Bransby & Springman 1997; Juirnarongrit & Ashford 2003; Armstrong et al. 2014). However, it was back-rotation that incurred failure of most of the piles during nature disasters (Knappett & Madabhushi 2009; Fraser 2013; Haskell et al. 2013, Guo 2020). The tests were conducted using the apparatus shown previously (Guo et al 2017) on 2 piles in line, without an axial loading P (= 0) or with P of 294 N/pile, respectively, at the sliding depth (SD) l_m of 0.57l (i.e. 0.4 m). The model piles were subjected to a uniform translation of the sand (at the

loading location, Fig .1) to a total movement w_f of 140 mm. The piles were made of aluminum tube, 1.2 m in length, 32 mm in diameter (d_{32}), and 1.5 mm in wall thickness (t). The bending stiffness E_pI_p is 1.28×10^6 kNmm^2. The model sand has a dry density γ' of 16.27 kN/m^3 and an internal (residual) frictional angle ϕ of 38°. The d_{32} piles were socketed into an aluminum cap. The bending capacity M_o^y of the pile-cap connections is 5–10% of the pile body (M_y). The tests provide profiles of bending moment, shear force, soil reaction, and deflection, and maximum bending moment M_m, maximum shear force Q_m, pile-rotation angle ω_r, and pile-head deflection w_g, and k_s of 20–35 kPa.

The model piles display features of sway, sliding and back-rotation, as with in-situ piles. The pile deflection w_g, rotation angle ω_r and bending moment need to be curbed to prevent formation of hinges. They are estimated as (Guo 2016) (i) k_s = 25 kPa (= 2.1G_s, and G_s = 12 kPa). (ii) m = 17.7 (= K_p/K_a, ultimate state). (iii) p_{ub} = 10 kN/m (= $s_g\gamma'K_p^2dl$), using γ' = 16.5 kN/m^3, ϕ = 38°, d = 32 mm, l = 0.7 m, and s_g = 1.53 (average). The p_{ub} and k_s values for rotating piles are reduced to 5.0–5.6 kN/m and 14–16 kPa, respectively to simulate translating piles. The parameters are 'identical' to those of forward rotating piles but a negative k_θ (with $\bar{k}_\theta$ = -0.04). They are presented together as m/k_s(kPa)/p_b(kN/m)/$\bar{k}_\theta$ of 17.7/25/5.6/-0.04, and 17.7/16/5/-0.04, respectively for no-loading and with vertical loading, respectively.

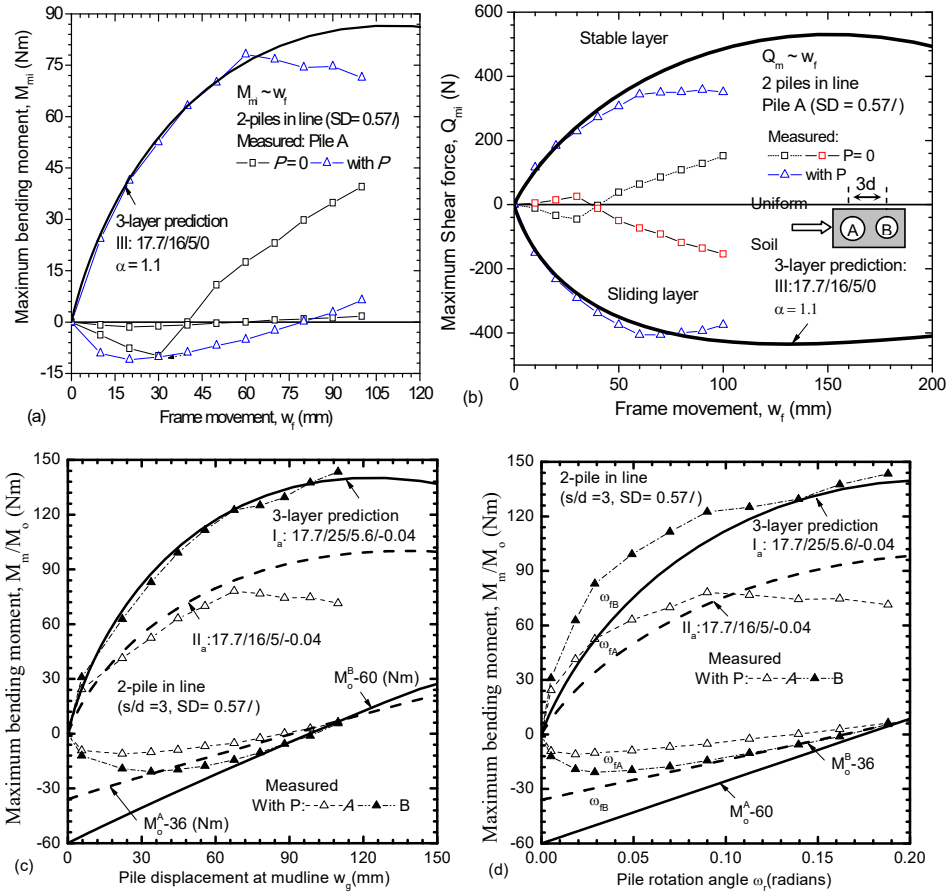

Figure 7: Yielding and sliding piles – Predicted versus measured development of 2-pile in-line groups: (a) $M_{mi} - w_f$, (b) $Q_{mi} - w_f$, (c) w_g–M_{mi}, and (d) ω_r–M_{mi}

The test piles are subjected to soil movement only and no shear force at head-level (with H = 0). The M_y is estimated grossly using yielding stress of 350 MPa (the aluminum) as 0.4 kNm [=$350\times10^3\times1.28/(70\times10^6)/(0.5d)$ m, d = 0.032 m, Young's modulus of 70 GPa]. The connection M_o^y (= $M_y\omega/\omega_r$) is estimated as 20–60 Nm using ω/ω_r = 0.05–0.2. The M_o^y/M_y ratio is much lower than 0.25–0.6 gained from steel pile-to pile-cap

connection due to stress concentration at the pile and cap connection.

6 CONCLUSIONS

This paper provides investigation into response of piles subjected to embankment loading, and backrotated piles in light of 2-/3-layer models. Recent advance is briefly reviewed concerning range of parameters used to model piles subjected to excavation and embankment loading. Simulations of six centrifuge tests on embankment piles are elaborated. 1g model tests are provided to reveal backrotation behaviour of piles, and its capture using a negative stiffness in the 2-/3- models. The study is aimed to unite the design piles under passive loading (e.g. lateral spreading, embankment, excavation, sliding slope, etc.).

7 REFERENCES

Armstrong, R. J., R. W. Boulanger & M. H. Beaty 2014. "Equivalent static analysis of piled bridge abutments affected by earthquake-induced liquefaction." *Journal of Geotechnical and Geoenvironmental Engineering, ASCE* 140(8): 04014046.

Bransby, M. F. & S. M. Springman 1997. Centrifuge modelling of pile groups adjacent to surcharge loads. *Soils and Foundations* 37(2): 39-49.

Dobry, R., T. Abdoun, T. D. O'Rourke & S. H. Goh 2003. Single piles in lateral spreads: field bending moment evaluation. *Journal of Geotechnical and Geoenvironmental Engineering, ASCE* 129(10):879-889.

Frank, R. & P. Pouget 2008. Experimental pile subjected to long duration thrusts owing to a moving slope. *Geotechnique* 58(8): 645-658.

Guo, W. D. 2012. *Theory and practice of pile foundations*. Boca Raton, London, New York, CRC press.

Guo, W. D. 2015. Nonlinear response of laterally loaded rigid piles in sliding soil. *Canadian Geotechnical Journal* 52(7): 903-925.

Guo, W. D. 2016. Response of rigid piles during passive dragging. *International Journal for Numerical and Analytical Methods in Geomechanics* 40(14): 1936-1967.

Guo, W. D., H. Y. Qin & E. H. Ghee 2017. Modeling single piles subjected to evolving soil movement. *International Journal of Geomechanics* 17(4): 180-196.

Haskell, J. J. M., S. P. G. Madabhushi, M. Cubrinovski & A. Winkley 2013. Lateral spreading-induced abutment rotation in the 2011 Christchurch earthquake: observation and analysis. *Geotechnique* 63(15):1310-1327.

Jeong, S., J. L. D. Seo & J. Park 1995. "Time-dependent behavior of pile groups by staged construction of an adjacent embankment on soft clay." *Canadian Geotechnical Journal* 41: 644-656.

JRA 2002. Specifications for highway bridges, Japan Road Association. Prepared by Public Works Research Institute (PWRI) and Civil Engineering Research Laboratory (CRL). Japan.

Knappett, J. A. & S. P. G. Madabhushi 2009. Influence of axial load on lateral pile response in liquefiable soils. Part II: numerical modelling. *Geotechnique* 59(7): 583-592.

Leung, C. F., Y. K. Chow & R. F. Shen 2000. "Behaviour of pile subject to excavation-induced soil movement." *Journal of Geotechnical and Geoenvironmental Engineering, American Society of Civil Engineers* 126(11), 947-954.

Ong, D. E. L., C. F. Leung, Y. K. Chow and T. G. Ng 2006. "Severe damage of a pile group due to slope failure." *Journal of Geotechnical and Geoenvironmental Engineering, American Society of Civil Engineers* 141(12): 04015014.

Stewart, D. P., R. J. Jewell & M. F. Randolph 1994. Design of piled bridge abutment on soft clay for loading from lateral soil movements. *Geotechnique* 44(2):277-296.

Xiao, Y., H. Wu, T. T. Yaprak, G. R. Martin & J. B. Mander 2006. Experimental studies on seismic behavior of steel pile-to-pile-cap connections. *J. Bridge Engrg. ASCE* 11(2): 151-159.